Neuro-Oncology Advances
4(1), 1–8, 2022 | https://doi.org/10.1093/noajnl/vdab167 | Advance Access date 18 November 2021

A functional artificial neural network for noninvasive pretreatment evaluation of glioblastoma patients

Eric Zander†, Andrew Ardeleanu†, Ryan Singleton†, Barnabas Bede, Yilin Wu, and Shuhua Zheng

Department of Mathematics, DigiPen Institute of Technology, Redmond, Washington, USA (E.Z., A.A., R.S., B.B., Y.W.); Department of General Surgery, San Joaquin General Hospital, French Camp, California, USA (S.Z.)

†These authors contributed equally to the this study.

Corresponding Author: Shuhua Zheng, DO, PhD, Department of General Surgery, San Joaquin General Hospital, French Camp, 95231, CA, USA (s.zheng1@med.miami.edu).

Abstract

Background. Pretreatment assessments for glioblastoma (GBM) patients, especially elderly or frail patients, are critical for treatment planning. However, genetic profiling with intracranial biopsy carries a significant risk of permanent morbidity. We previously demonstrated that the *CUL2* gene, encoding the scaffold cullin2 protein in the cullin2-RING E3 ligase (CRL2), can predict GBM radiosensitivity and prognosis. *CUL2* expression levels are closely regulated with its copy number variations (CNVs). This study aims to develop artificial neural networks (ANNs) for pretreatment evaluation of GBM patients with inputs obtainable without intracranial surgical biopsies.

Methods. Public datasets including Ivy-GAP, The Cancer Genome Atlas Glioblastoma (TCGA-GBM), and the Chinese Glioma Genome Atlas (CGGA) were used for training and testing of the ANNs. T1 images from corresponding cases were studied using automated segmentation for features of heterogeneity and tumor edge contouring. A ratio comparing the surface area of tumor borders versus the total volume (SvV) was derived from the DICOM-SEG conversions of segmented tumors. The edges of these borders were detected using the canny edge detector. Packages including Keras, Pytorch, and TensorFlow were tested to build the ANNs. A 4-layered ANN (8-8-8-2) with a binary output was built with optimal performance after extensive testing.

Results. The 4-layered deep learning ANN can identify a GBM patient's overall survival (OS) cohort with 80%–85% accuracy. The ANN requires 4 inputs, including *CUL2* copy number, patients' age at GBM diagnosis, Karnofsky Performance Scale (KPS), and SvV ratio.

Conclusion. Quantifiable image features can significantly improve the ability of ANNs to identify a GBM patients' survival cohort. Features such as clinical measures, genetic data, and image data, can be integrated into a single ANN for GBM pretreatment evaluation.

Key Points

- This study establishes a noninvasive pretreatment evaluation of GBM patients.
- Artificial neural network (ANN) performs deep learning with 4 inputs.
- ANN facilitates GBM prognosis prediction and can guide treatment planning.

Glioblastoma (GBM) is an aggressive form of tumor in the central nervous system (CNS), with less than 5% of patients surviving for 5 years following initial diagnosis.[1] While concurrent and adjuvant chemoradiotherapy constitutes standardized treatment for GBM after the Stupp et al. clinical trial in 2005, finding methods of refining treatment planning are urgently needed for better clinical outcomes.[2] Furthermore, treatment for elderly and frail GBM patients is not standardized as they were

Importance of the Study

Pretreatment evaluation is critical for personalized GBM treatment planning, particularly for those frail and elderly patients. Artificial neural network (ANN) provides a unique opportunity to integrate critical information from different clinical aspects to facilitate the decision-making process right at the diagnosis of the GBM. This study provides a model of ANN that uses 4 simple inputs, that is, *CUL2* copy number, Karnofsky Performance Scale (KPS), age at GBM diagnosis, and surface versus volume (SvV) ratio of T1 MRI, all of which are obtainable without intracranial interventions. This study offers a new perspective in how to incorporate recent development of machine learning (ML) in better cancer patient care.

excluded in the Stupp et al. trial.[2] Therefore, pretreatment evaluation is extremely valuable in guiding the selection of treatment options.

Recent advances on GBM radiomics as well as machine learning (ML) applications in neuroimaging analysis promises a personalized treatment strategy that can lead to the paradigm shift for GBM management.[3,4] Aspects of deep learning (DL), a subfield of ML concerned with multilayered ANNs, stand to benefit GBM research in particular given that applications in incorporating medical image processing and genetic data mining.[4–6] However, acquisition of genetic data, including RNA-sequence (RNA-Seq), isocitrate dehydrogenase (*IDH*) mutation, and cytosine-phosphate-guanine (CpG) island methylator phenotype (G-CIMP) status, requires intracranial biopsy which carries a significant risk of perioperative complication.[7] Therefore, a noninvasive method is urgently needed in the presurgical evaluation of GBM patients, particularly for those elderly and frail.[8,9]

We recently demonstrated that expression levels of *CUL2*, which encodes the cullin2 scaffold protein in the cullin2-RING E3 ligase (CRL2) complex, can predict GBM radiosensitivity and prognosis.[10] CRL2 is the E3 ligase that degrades critical proteins such as hypoxia-inducible factor 1 (HIF-1) α that is involved in GBM neovascularization, and epidermal growth factor receptor (EGFR) that is involved in GBM progression.[10] *CUL2* copy number variation (CNV) dictates expression levels, suggesting that models could rely on CNVs measured through noninvasive methods rather than expression levels to predict patients' survival rates.[10,11] In this study, we attempted to integrate quantifiable image data, genetic information such as *CUL2* CNVs, and clinical data such as Karnofsky Performance Scale (KPS) in a functional ANN for noninvasive presurgical evaluation GBM patients.

Materials and Methods

Public Datasets

Datasets including genetic data regarding *CUL2* CNVs and expression levels, clinical data indicating patient demographic and overall survival (OS), and T1 magnetic resonance imaging (MRI) images enabled this study. Such datasets include The Cancer Genome Atlas Glioblastoma (TCGA-GBM), the Ivy Glioblastoma Atlas Project (Ivy-GAP), and the Chinese Glioma Genome Atlas (CGGA).[12–14] Clinical and genetic data from the TCGA-GBM were acquired through the Xena platform (https://xena.ucsc.edu/).[15] TCGA-GBM images were made available through The Cancer Imaging Archive (TCIA).[16] This also includes skull-stripped and co-registered segmentations of TCGA-GBM images made available by Bakas et al., as well as DICOM-SEG conversions of these segmented images created by Beers et al.[16] Images from the Ivy-GAP dataset were also acquired through TCIA, with clinical and genetic data made available by Puchalski et al.[13]

T1 MRI Image Segmentation

While images considered in this research included post-gadolinium T1-weighted DICOM images from the original TCGA-GBM dataset, the features used in modeling were derived from the most voluminous DICOM-SEG conversions of images in the segmented image dataset for each patient. Python packages for processing image files in the DICOM, DICOM-SEG, and NIfTI file formats include pydicom, pydicom_seg, and nibabel, respectively.

Image Analyses

To explore the value of image features in forecasting patient outcomes, a ratio comparing the surface area of tumor borders to the total volume of borders was derived from the DICOM-SEG conversions of segmented tumors. The edges of these borders can be detected using the canny edge detector such as the one available from the Skimage, or Scikit-image, Python package. Finding the sum of the pixels forming these edges gives a close approximation of surface area. Tumor border volume can be calculated by summing up all pixels within the tumor borders. Calculating the tumor surface area versus volume (SvV) ratio between the two is then as simple as dividing the surface area by volume (SvV = Surface Area/Volume). This results in a value unique to each patient that is indicative of tumor border regularity.[17]

Kaplan–Meier (K–M) Survival Analysis

K–M survival analyses for GBM with differential *CUL2* copy numbers, KPS rankings, age at GBM diagnosis, surface area, and SvV ratios were conducted using the Lifelines

library. The data set is split into two at the mean value of any of respective attributes above. Any value above the mean for that attribute is placed in the upper group, while any value below the mean is placed in the lower group. Therefore, the number of patients in either group varies from attribute to attribute. The number of patients in any one group is labeled next to the legend for that group on its graph. Log-Rank analyses for *P*-values smaller than .05 were considered statistically significant.

ANN of GBM Genomics and Clinical Features

Four different ANNs were created for the purpose of predicting patients' OS cohort and to test whether measuring patient *CUL2* copy numbers would yield similar results to *CUL2* expression levels. Results are determined by how often a neural network can identify a patient's OS cohort based on clinical data. Four different loss functions were used to test on all 4 of our neural networks, resulting in 16 different results to compare. The loss functions we chose were Binary Crossentropy, Mean Absolute Error, Mean Error Squared, and Categorical Crossentropy. The packages used for creating these neural networks include Keras, Pytorch, and TensorFlow. After extensive testing, a 4-layer model (8-8-8-2), with a binary output, was built. The first layer consists of 8 nodes and takes number of inputs based on the information we are passing to it. The groups of information being passed to our neural networks are as follows: Baseline (Age, KPS, longest dimension), Expression (*CUL2* expression, Age, KPS, longest dimension), CNV (*CUL2* copy numbers, Age, KPS, longest dimension), and Feature Data (*CUL2* copy numbers, Age, SvV). Each neural network consequently requires different numbers of inputs. The second and third layer feature 8 nodes and employ a ReLU activation function. Finally, the output layer is binary.

The output layer of the ANN splits each dataset into OS cohorts. Patients who are assigned a "1" survived longer, and those who did not are assigned a "0." The data are split to be approximately 55%–45% in favor of "0" targets, with the exception of the feature dataset which is split approximately 60%–40% in favor of "0" targets. This is to ensure a balance of training and testing datasets with the relevant features. Figure 3A is a schematic overview of the architecture of the ANN.

Results

CUL2 CNVs and GBM Genotype

Copy number loss of chromosome (chr) 10 is one of the initial driver events of non-cytosine-phosphate-guanine (CpG) island methylator phenotype (non-G-CIMP) GBM tumorigenesis.[18] In GBM patients (n = 576) derived from TCGA dataset, we found that copy number loss of *CUL2*, located in chr10p11 (chr10p), is related with non-G-CIMP, *IDH1* wildtype ($IDH1^{WT}$) GBM (Figure 1A). *IDH1* mutations status and G-CIMP positivity are key genotypic biomarkers critical for GBM classification, prognosis, and treatment planning.[19] Therefore, these results indicate that *CUL2* copy numbers can reflect the fundamental genetic background of GBM. *CUL2* CNVs have a strong positive correlation with its expression levels in GBM (Figure 1A). We went further to study the correlation of *CUL2* CNVs and expression in other cell types derived from both cranial and extracranial tissue. We found linear correlation between *CUL2* CNVs and expression levels in cancer cell lines derived from cranial (eg, glioma, medulloblastoma, meningioma) and extracranial (eg, B-/T-cell leukemia, multiple myeloma, small cell lung cancer [SCLC], pancreatic cancer, soft tissue, breast cancer, thyroid cancer) tissues (Figure 1B). Notably, the linear correlation between *CUL2* CNVs and expressions levels in pancreatic cancer and SCLC exhibit a coefficient of determination (R^2) (0.71 and 0.78, respectively) and may be described by equations (y = 1.021*x+ 3.4467 and y = 1.288*x + 3.7066, respectively). These relationships prove similar to those in glioma cancer cells (R^2 = 0.71, y = 1.15*x + 3.6955) (Figure 1C–E). This elucidates the valuable linear relationship between *CUL2* CNVs and expression levels. *CUL2* levels in extracranial tissue may also reflect expression levels in central neural system (CNS) malignancies.

GBM T1 MRI Segmentation and Tumor Surface Regularity

Many radiomic features serve as predictors for GBM OS rates.[20] These include attributes such as first order statistics, texture features, and data describing the shape of the tumor. One method of systematically measuring shape involves finding the SvV of tumor borders.[21] Using the most voluminous binary segmentation masks attainable from DICOM-SEG (DSO) conversions for the TCGA-GBM segmentation dataset for each patient, the surface areas of tumor borders were approximated by summing the number of pixels belonging to edges of 2D slices determined via canny edge detection (Figure 2A). The volumes of segmented tumors masks were then approximated by summing up all pixels of each slice (Figure 2A). Applying this approach on the segmented image dataset creates surface area (S), volume (V), and SvV ratio data for 102 patients, 98 of these patients have *CUL2* CNV data. We found the correlation of S and V with equation $S = 3.5887*V^{0.7228}$ (R^2 = 0.8346) (Figure 2C). Calculation of partial derivative of the equation gets the equation $\partial s/\partial v = 2.59391*v^{-0.2772}$ (Figure 2B,C). These results indicate that SvV ratios provide unique feature to GBM patients (Figure 2B,C).

Segmented Image Features

To further investigate the clinical relevance of proposed segmentation methods, we studied the prognostic value of quantifiable image features in GBM. These features include the total surface area, tumor volume and SvV ratio. In Kaplan–Meier analyses where median values are used as cutoffs, we found no difference in OS between groups with High and Low values for surface, volume and SvV values (Supplementary Figure 1). However, given that each parameter in the MRI images is unique for individual GBM patient, we tested these image features as additional inputs in our neural network to evaluate their predictive value.

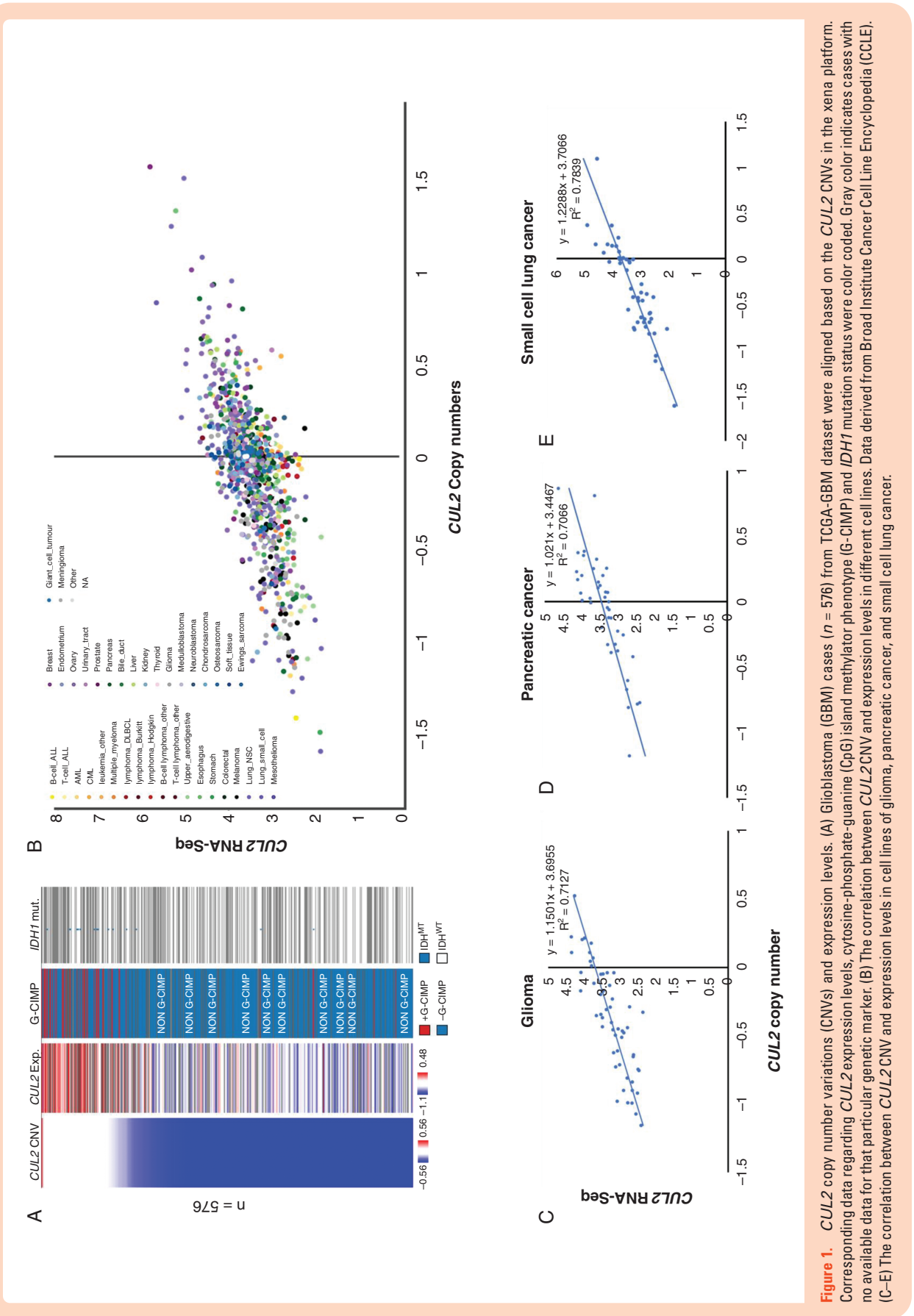

Figure 1. *CUL2* copy number variations (CNVs) and expression levels. (A) Glioblastoma (GBM) cases ($n = 576$) from TCGA-GBM dataset were aligned based on the *CUL2* CNVs in the xena platform. Corresponding data regarding *CUL2* expression levels, cytosine-phosphate-guanine (CpG) island methylator phenotype (G-CIMP) and *IDH1* mutation status were color coded. Gray color indicates cases with no available data for that particular genetic marker. (B) The correlation between *CUL2* CNV and expression levels in different cell lines. Data derived from Broad Institute Cancer Cell Line Encyclopedia (CCLE). (C–E) The correlation between *CUL2* CNV and expression levels in cell lines of glioma, pancreatic cancer, and small cell lung cancer.

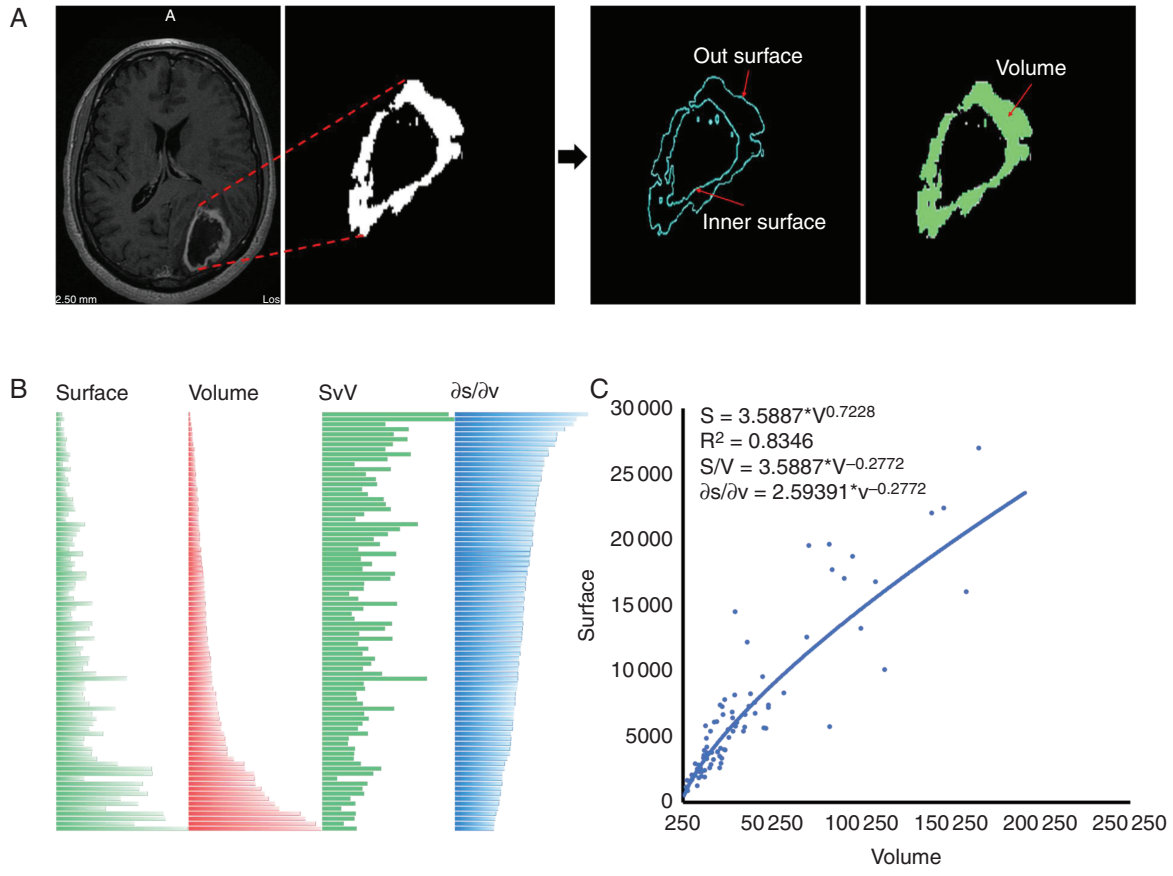

Figure 2. Glioblastoma (GBM) T1 image segmentation. (A) Example of binary segmentation masks attainable from DICOM-SEG (DSO) conversions for the TCGA-GBM dataset. The surface area of tumor borders calculated by summing up edges of 2D slices derived with a canny edge detector. The volumes were approximated by summing up all pixels of each slice. (B) GBM cases ($n = 84$) were aligned based on increasing volume. The surface area, surface versus volume (SvV), and partial derivative ∂s/∂v were aligned accordingly. (C) Relationship between surface area and volume of GBM based on segmented images ($n = 84$).

Constructed ANNs Indicate Likely GBM Survival Cohort

The chosen loss function may afford or disallow optimal ANN performance depending on the nature of the problem.[22] To find an appropriate loss function for the classification of a patient's OS cohort, we tested 4 different loss functions on 4 neural networks. This resulted in 16 different results to compare. The loss functions we tested included Binary Crossentropy, Mean Absolute Error, Mean Error Squared, and Categorical Crossentropy (Supplementary Figure 2).[22] The structure of the ANN we chose is a 4-layer model (8-8-8-2), with a binary output (Figure 3A). Due to limited cases with image data to calculate SvV, we used the longest dimension of GBM tumor mass as an input in certain ANNs. The first layer consists of 8 nodes with sets of inputs as follows: Baseline dataset (age, KPS, longest dimension), Expression dataset (*CUL2* expression, age, KPS, longest dimension), CNV dataset (*CUL2* copy numbers, age, KPS, longest dimension), and Feature Data dataset (*CUL2* copy numbers, age, SvV) (Supplementary Figure 2). The second and third layer are also 8 nodes with a rectified linear activation function (ReLU). The last layer features binary output. Patients who are assigned a "1" will likely exhibit greater OS, and those who are assigned a "0" will not (Figure 3A). As expected, the Baseline neural network with fewer features performed poorest in all 4 trials (Supplementary Figure 2). We found the CNV neural network slightly outperformed the Expression neural network (Supplementary Figure 2, Figure 3C). Therefore, *CUL2* expression levels or *CUL2* copy numbers will yield similar results, with around 75% accuracy as displayed on the average of the 4 loss functions combined in a single visual (Figure 3C). Employing image feature data as inputs afforded the greatest performance of about 80%–85% (Figure 3C).

To achieve these results and identify the set of inputs that produce the best performing ANN, we performed a set number of trials for each of our 16 neural networks. Each of the ANNs were run 1000 times for a total of 16,000 trials and 16 ANNs. The best performing model for each input was saved for the purpose of distribution and to view the model's structure and weights. To reiterate, the best performing ANN employed the

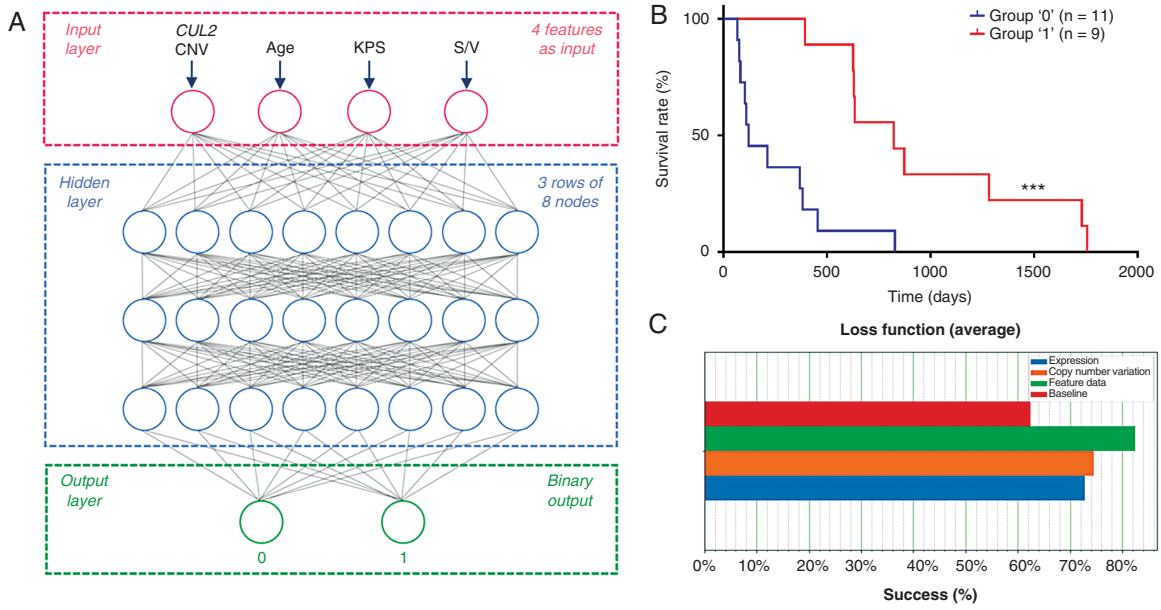

Figure 3. Parameterizing artificial neural networks (ANNs) based on *CUL2* copy number variations (CNVs), image features and clinical data. (A) A schematic overview of the 4-layer neural networks with the Feature Data with inputs of *CUL2* copy numbers, age at glioblastoma (GBM) diagnosis, and SvV. (B) Kaplan–Meier analysis of the test set of GBM cases assigned by the Feature Data-based neural network to group "1" and "0". (C) Average performance of 4 neural networks based on 4 set of inputs including baseline (age, Karnofsky Performance Scale [KPS], longest dimension), expression (*CUL2* expression, age, KPS, longest dimension), CNV (*CUL2* copy numbers, age, KPS, longest dimension), and feature data (*CUL2* copy numbers, age, KPS, SvV).

Feature Data dataset with *CUL2* copy numbers, Age, and SvV to allow a consistent 80%–85% accuracy across all loss functions (Supplementary Figure 2, Figure 3C). The Kaplan–Meier survival analysis for the test set of 20 GBM patients in the Feature Data group was presented ($P = .0005$; Figure 3B).

Discussion

We previously demonstrated that one may evaluate *CUL2* gene expression levels and CNVs to predict radiosensitivity and overall survival (OS) in GBM patients.[10] This study explored the potential value of this concept to the training of ANNs and deep learning (DL) of clinical information, T1 MRI-based imaging features, and *CUL2* copy numbers in pretreatment evaluation. In our best performing ANN, we consistently identified the OS cohort of GBM patients with accuracies of 80%–85% using *CUL2* copy numbers, patients' ages at GBM diagnosis, and SvV ratio in segmented images as inputs. All these inputs are objective quantifiable parameters that can be obtained without any intracranial biopsy which carries significant risk of causing serious permanent morbidity (5%).[7] Therefore, our model provides a unique tool for noninvasive presurgical evaluation of GBM patients regarding prognosis, which will be of great value for treatment planning.

We found the usage of tumor border surface area and volume led to improved accuracy for each ANN model. This not only suggests that the uniqueness of these measurements, but also illustrates the general value of quantifiable features derived from image processing in anticipating treatment outcomes. In addition to including other measurements of shape indicating surface regularity, future models could also potentially integrate first order statistics regarding gray level intensity, textural features, and a myriad of radiomic features with demonstrable impact on GBM survival. Artificial intelligence-based automated image segmentation will play a critical role in this aspect.

Processing medical images such as T1 images involves numerous challenges, but several approaches exist to extract hundreds of potentially useful features of each category. Image processing solutions that employ convolutional neural network architectures such as 3D U-Net to automate tumor segmentation allow the systematic tumor segmentation, though atlas. Ultimately, additional image features derived using DL solutions stand to improve the already promising model by introducing more noninvasive data alongside *CUL2* CNVs, further indicating the value of combining such measurements to predictions concerning treatment response.

Although we built a promising model for noninvasive presurgical evaluation of GBM patients, several steps may be performed to further test and enhance these findings. Firstly, the incorporation of additional image features would likely improve the predictive value of our existing neural networks. Secondly, solely leveraging data from select prior studies for both training and testing may limit

generalizability. Clinical trial and additional testing of the model on other cohorts would assist in validating whether the given ANNs can guide RT treatment planning in future contexts. Furthermore, the reliance on subjective clinical parameters may introduce unnecessary risk. Developing neural networks that perform consistently with only imaging data and patients' age would markedly improve the value of such models. Finally, the value of the discussed model is limited by the binary output layer. Future models developed with additional data could support a higher resolution of output and bolster treatment planning.

In summary, the previously established relationship between *CUL2* CNVs and clinically significant attributes such as radiosensitivity prompted the testing of ANNs capable of aiding in pretreatment evaluation. Noninvasive clinical, genetic, and image data were leveraged in training to afford the ability to identify a patient's OS cohort with accuracies of 80%–85%. The best performing model consistently achieved these scores by training with *CUL2* CNVs, patient age, and tumor surface area versus volume. Further testing with additional cohorts and the introduction of additional image features may improve generalizability, enhance output resolution, and afford greater accuracy. Nonetheless, the given model stands to both assist GBM pretreatment evaluation and demonstrate the value of DL in the relevant decision-making processes.

Supplementary Material

Supplementary data are available at *Neuro-Oncology Advances* online.

Keywords

artificial intelligence | copy number variations | cullin2 | glioblastoma | machine learning.

Funding

None declared.

Authorship Statement. All authors reviewed the literature, contributed to data interpretation, and read and approved the final article. S.H.Z., Y.L.W., and B.B. conceptualized the study. S.H.Z., Y.L.W., B.B., E.Z., A.A., and R.S. designed the study. S.H.Z., E.Z., A.A., and R.S. collected the data. E.Z., A.A., and R.S. developed the algorithm and S.H.Z., E.Z., A.A., and R.S. analyzed the data. H.Z., Y.L.W., B.B., E.Z., A.A., and R.S. drafted the article. H.Z., Y.L.W., B.B., E.Z., A.A., and R.S. critically revised the article.

Conflict of interest statement. None declared.

References

1. Ostrom QT, Cioffi G, Gittleman H, et al. CBTRUS statistical report: primary brain and other central nervous system tumors diagnosed in the United States in 2012-2016. *Neuro Oncol* 2019; 21(Supplement_5): v1–v100.
2. Stupp R, Mason WP, van den Bent MJ, et al.; European Organisation for Research and Treatment of Cancer Brain Tumor and Radiotherapy Groups; National Cancer Institute of Canada Clinical Trials Group. Radiotherapy plus concomitant and adjuvant temozolomide for glioblastoma. *N Engl J Med.* 2005;352(10):987–996.
3. Zhang X, Lu H, Tian Q, et al. A radiomics nomogram based on multiparametric MRI might stratify glioblastoma patients according to survival. *Eur Radiol.* 2019;29(10):5528–5538.
4. Havaei M, Davy A, Warde-Farley D, et al. Brain tumor segmentation with Deep Neural Networks. *Med Image Anal.* 2017;35:18–31.
5. Yan JL, Li C, van der Hoorn A, Boonzaier NR, Matys T, Price SJ. A neural network approach to identify the peritumoral invasive areas in glioblastoma patients by using MR radiomics. *Sci Rep.* 2020;10(1): 9748.
6. Kamnitsas K, Ledig C, Newcombe VFJ, et al. Efficient multi-scale 3D CNN with fully connected CRF for accurate brain lesion segmentation. *Med Image Anal.* 2017;36:61–78.
7. McGirt MJ, Woodworth GF, Coon AL, et al. Independent predictors of morbidity after image-guided stereotactic brain biopsy: a risk assessment of 270 cases. *J Neurosurg.* 2005;102(5):897–901.
8. Wang Y, Zhao B, Chen W, et al. Pretreatment geriatric assessments of elderly patients with glioma: development and implications. *Aging Dis.* 2020;11(2):448–461.
9. Roa W, Kepka L, Kumar N, et al. International atomic energy agency randomized phase III study of radiation therapy in elderly and/or frail patients with newly diagnosed glioblastoma multiforme. *J Clin Oncol.* 2015;33(35):4145–4150.
10. Zheng S, Wu Y, Li Z. Integrating cullin2-RING E3 ligase as a potential biomarker for glioblastoma multiforme prognosis and radiosensitivity profiling. *Radiother Oncol* 2020;154:36–44.
11. Wong KK, deLeeuw RJ, Dosanjh NS, et al. A comprehensive analysis of common copy-number variations in the human genome. *Am J Hum Genet.* 2007;80(1):91–104.
12. Zhao Z, Meng F, Wang W, Wang Z, Zhang C, Jiang T. Comprehensive RNA-seq transcriptomic profiling in the malignant progression of gliomas. *Sci Data.* 2017;4:170024.
13. Puchalski RB, Shah N, Miller J, et al. An anatomic transcriptional atlas of human glioblastoma. *Science.* 2018;360(6389):660–663.
14. Brennan CW, Verhaak RG, McKenna A, et al.; TCGA Research Network. The somatic genomic landscape of glioblastoma. *Cell.* 2013;155(2):462–477.
15. Goldman MJ, Craft B, Hastie M, et al. Visualizing and interpreting cancer genomics data via the Xena platform. *Nat Biotechnol.* 2020;38(6):675–678.
16. Clark K, Vendt B, Smith K, et al. The Cancer Imaging Archive (TCIA): maintaining and operating a public information repository. *J Digit Imaging.* 2013;26(6):1045–1057.
17. Itakura H, Achrol AS, Mitchell LA, et al. Magnetic resonance image features identify glioblastoma phenotypic subtypes with distinct molecular pathway activities. *Sci Transl Med.* 2015;7(303):303ra138.
18. Ozawa T, Riester M, Cheng YK, et al. Most human non-GCIMP glioblastoma subtypes evolve from a common proneural-like precursor glioma. *Cancer Cell.* 2014;26(2):288–300.

19. Malta TM, de Souza CF, Sabedot TS, et al. Glioma CpG island methylator phenotype (G-CIMP): biological and clinical implications. *Neuro Oncol.* 2018;20(5):608–620.
20. Carré A, Klausner G, Edjlali M, et al. Standardization of brain MR images across machines and protocols: bridging the gap for MRI-based radiomics. *Sci Rep.* 2020;10(1):12340.
21. Pérez-Beteta J, Molina-García D, Ortiz-Alhambra JA, et al. Tumor surface regularity at MR imaging predicts survival and response to surgery in patients with glioblastoma. *Radiology.* 2018;288(1):218–225.
22. Ghodrati V, Shao J, Bydder M, et al. MR image reconstruction using deep learning: evaluation of network structure and loss functions. *Quant Imaging Med Surg.* 2019;9(9):1516–1527.